Femtosecond Infrared Study of the Dynamics of Solvation and Solvent Caging

Haw Yang,‡ Preston T. Snee, Kenneth T. Kotz, Christine K. Payne, and Charles B. Harris*

Contribution from the Department of Chemistry, University of California, Berkeley, California 94720, and Chemical Sciences Division, Ernest Orlando Lawrence Berkeley National Laboratory, Berkeley, California 94720

Received September 11, 2000

Abstract: The ultrafast reaction dynamics following 295-nm photodissociation of $Re_2(CO)_{10}$ were studied experimentally with 300-fs time resolution in the reactive, strongly coordinating CCl_4 solution and in the inert, weakly coordinating hexane solution. Density-functional theoretical (DFT) and ab initio calculations were used to further characterize the transient intermediates seen in the experiments. It was found that the quantum yield of the Re−Re bond dissociation is governed by geminate recombination on two time scales in CCl_4, ∼50 and ∼500 ps. The recombination dynamics are discussed in terms of solvent caging in which the geminate $Re(CO)_5$ pair has a low probability to escape the first solvent shell in the first few picoseconds after femtosecond photolysis. The other photofragmentation channel resulted in the equatorially solvated dirhenium nonacarbonyl *eq*-$Re_2(CO)_9$(solvent). Theoretical calculations indicated that a structural reorganization energy cost on the order of 6−7 kcal/mol might be required for the unsolvated nonacarbonyl to coordinate to a solvent molecule. These results suggest that for $Re(CO)_5$ the solvent can be treated as a viscous continuum, whereas for the $Re_2(CO)_9$ the solvent is best described in molecular terms.

Introduction

The reactivity of multinuclear compounds can generally be photochemically activated, creating one or multiple coordinatively vacant sites at the metal.[1] Dinuclear metal complexes such as $MM'(CO)_{10}$ (M, M′ = Mn, Re) can be viewed as prototypical compounds for organometallics of higher nuclearity in potential catalytic applications.[2−4] The primary photochemical reaction of $MM'(CO)_{10}$ in solution has been shown to result in (i) homolytic fission of the metal−metal σ-bond to form $M(CO)_5$ radicals, (ii) dissociation of a CO ligand to form $MM'(CO)_9$, and (iii) nondissociative relaxation to the electronic ground state:[2,5−8]

$$(CO)_5M-M'(CO)_5 \underset{(iii)}{\overset{h\nu}{\rightleftharpoons}} \begin{cases} M(CO)_5 + M'(CO)_5 & (i) \\ MM'(CO)_9 + CO & (ii) \end{cases} \quad (1)$$

The branching ratios have been found to depend on the excitation wavelength by which pathway (i) is favored by lower energy excitation whereas pathway (ii) is favored by higher energy excitation.[9−12] Experimentally, the short-lived photofragments $MM'(CO)_9$ and $M(CO)_5$ have been identified and characterized in the gas phase,[12,13] in low-temperature matrix isolation studies,[14−19] in liquid Xe,[17] and in room-temperature solutions.[7,20−22] These studies have been instrumental in establishing our current understanding of the photochemistry of $MM'(CO)_{10}$. However, the influence of the surrounding solvent over reaction pathways (i), (ii), and (iii) remains to be characterized. This work examines how the solvent participates in the chemical processes that follow photofragmentation of $Re_2(CO)_{10}$.

For $Re_2(CO)_{10}$ a UV pulse may cleave the Re−Re bond to form two formally 17-electron $Re(CO)_5$ radicals or the UV pulse may remove a CO ligand to form the coordinatively unsaturated $Re_2(CO)_9$. The chemistry that follows the generation of the reactive species $Re(CO)_5$ or $Re_2(CO)_9$ is quite different. The rhenium pentacarbonyl $Re(CO)_5$ that follows dissociation

* To whom correspondence should be addressed. E-mail: harris@socrates.berkeley.edu.

‡ Present address: Harvard University, Chemical Laboratories, Box 225, 12 Oxford St., Cambridge, MA 02138.

(1) Nakamura, A.; Tsutsui, M. *Principals and Applications of Homogeneous Catalysis*; John Wiley & Sons: New York, 1980.
(2) Meyer, T. J.; Caspar, J. V. *Chem. Rev.* **1985**, *85*, 187.
(3) Serpone, N.; Pelizzetti, E. *Photocatalysis*—Fundamentals and Applications; Wiley: New York, 1989.
(4) Adams, R. D.; Cotton, F. A. *Catalysis by Di- and Polynuclear Metal Cluster Complexes*; Wiley VCH: New York, 1998.
(5) Wrighton, M.; Bredesen, D. *J. Organomet. Chem.* **1973**, *50*, C35.
(6) Wegman, R. W.; Olsen, R. J.; Gard, D. R.; Faulkner, L. R.; Brown, T. L. *J. Am. Chem. Soc.* **1981**, *103*, 6089.
(7) Church, S. P.; Hermann, H.; Grevels, F.; Schaffner, K. *J. Chem. Soc., Chem. Commun.* **1984**, 785.
(8) Firth, S.; Hodges, P. M.; Poliakoff, M.; Turner, J. J.; Therien, M. J. *J. Organomet. Chem.* **1987**, *331*, 347.
(9) Wrighton, M. S.; Ginley, D. S. *J. Am. Chem. Soc.* **1975**, *97*, 2065.
(10) Gard, D. R.; Brown, T. L. *J. Am. Chem. Soc.* **1982**, *104*, 6340.
(11) Kobayashi, T.; Ohtani, H.; Noda, H.; Teratani, S.; Yamazaki, H.; Yasufuku, K. *Organometallics* **1986**, *5*, 110.
(12) Seder, T. A.; Church, S. P.; Weitz, E. *J. Am. Chem. Soc.* **1986**, *108*, 7518.
(13) Freedman, A.; Nersohn, R. *J. Am. Chem. Soc.* **1978**, *100*, 4116.
(14) Hepp, A. F.; Wrighton, M. S. *J. Am. Chem. Soc.* **1983**, *105*, 5934.
(15) Dunkin, I. R.; Harter, P.; Shields, C. J. *J. Am. Chem. Soc.* **1984**, *106*, 7248.
(16) Firth, S.; Hodges, P. M.; Poliakoff, M.; Turner, J. J. *Inorg. Chem.* **1986**, *25*, 4608.
(17) Firth, S.; Klotzbuecher, W. E.; Poliakoff, M.; Turner, J. J. *Inorg. Chem.* **1987**, *26*, 3370.
(18) Church, S. P.; Poliakoff, M.; Timney, J. A.; Turner, J. J. *J. Mol. Struct.* **1982**, *80*, 159.
(19) Huber, H.; Kunding, E. P.; Ozin, G. A. *J. Am. Chem. Soc.* **1974**, *96*, 5585.
(20) Rothberg, L. J.; Cooper, N. J.; Peters, K. S.; Vaida, V. *J. Am. Chem. Soc.* **1982**, *104*, 3536.
(21) Zhang, J. Z.; Harris, C. B. *J. Chem. Phys.* **1991**, *95*, 4024.
(22) Owrutsky, J. C.; Baronavski, A. P. *J. Chem. Phys.* **1996**, *105*, 9864.

10.1021/ja003344y CCC: $20.00
Published on Web 04/12/2001

pathway (i) has been shown to assume a C_{4v}, square-pyramidal geometry from solid CO matrix studies.[18,19] Such a 17-electron $Re(CO)_5$ radical is capable of abstracting a halogen atom from halogenated alkanes.[23,24] This type of one-electron oxidative addition to a metal center has been thought to be one of the crucial steps in many catalytic reactions.[25] One of the central questions regarding the reactivity of 17-electron species is the possible involvement of a 19-electron precursory complex of the form $(CO)_5Re\cdots Cl-CR_3$ during the course of reaction. This question has been addressed in a recent study and it was found that for the abstraction of a Cl atom from CH_nCl_{4-n} by $Re(CO)_5$, the rhenium radical is best viewed as an unsolvated 17-e^- species.[26] Due to the weak interaction between a $Re(CO)_5$ radical and the surrounding solvent molecules, a geminate $Re(CO)_5$ radical pair may recombine to reform the parent $Re_2(CO)_{10}$ molecule on an ultrafast time scale. It will be shown that for this dissociation pathway, the competition of Cl-abstraction and geminate recombination is regulated by solvent caging.

For dissociation pathway (ii), Firth et al. have shown in a low-temperature study that the primary photoproduct $Re_2(CO)_9$ has a coordinatively vacant site in the equatorial position, denoted *eq*-$Re_2(CO)_9$.[17] Irradiation with 546-nm light converts *eq*-$Re_2(CO)_9$ to the other isomer *ax*-$Re_2(CO)_9$ with an axial vacant site. One possible reaction following CO photolysis is ligand substitution at the vacant site of $Re_2(CO)_9$. Coville and co-workers have studied a series of substituted $Re_2(CO)_9L$ (L = ligand) and concluded that there is a delicate balance in the electronic and steric effects in the relative stability of the axially or equatorially substituted isomers.[27−29] In room-temperature solutions, it is observed that a solvent molecule enters the coordinatively vacant site to form a solvated complex $Re_2(CO)_9$-(solvent) within a few picoseconds following photodissociation. However, as will be shown later, such solvation may require structural reorganization of the $Re_2(CO)_9$ metal fragment. If the complexation energy of a solvent molecule and the metal center is not sufficient to compensate for the energy cost for structural reorganization, the unsolvated $Re_2(CO)_9$ complex may appear thermodynamically more stable in weak-coordinating solvents. For instance, the unsolvated *eq*-$Re_2(CO)_9$ complex has been observed in the Ar and N_2 matrices.[17] With the aid of quantum-chemical calculations, the picture of reorganization/solvation will be used to explain the experimental results.

Methods

Samples. Dirhenium decacarbonyl $Re_2(CO)_{10}$ (98%) and carbon tetrachloride CCl_4 (99.9%, d = 1.589 g/cm^3) were purchased from Aldrich, Inc. Hexane (C_6H_{14}, 99.9%, d = 0.664 g/cm^3), trichloromethane ($CHCl_3$, 99%, d = 1.484 g/cm^3), and dichloromethane (CH_2Cl_2, 99.9%, d = 1.3255 g/cm^3) were purchased from Fisher Scientific, Inc. All chemicals were used without further purification. The sample was enclosed in an airtight, demountable liquid IR flow cell (Harrick Scientific Corporation). The concentrations of the $Re_2(CO)_{10}$ solutions were approximately 7 mM in hexanes and 4 mM in chlorine-substituted methanes.

Femtosecond Infrared Spectroscopy. Details of the femtosecond IR (fs-IR) spectrometer setup have been published elsewhere.[30] Briefly, the output of a Ti:sapphire oscillator was amplified in a series of dye amplifiers pumped by a 30-Hz Nd:YAG laser. The UV and IR beams used to initiate and probe the reaction were generated through nonlinear crystals. The resulting 295-nm UV photons (with energy of ~5 μJ/pulse) were focused into a disk of ~200 μm diameter at the sample to initiate chemical reactions. The ~1-μJ IR pulses having a temporal full-width-half-maximum of about 70 fs and a spectral bandwidth of about 200 cm^{-1} were split into a signal and a reference beam to minimize the shot-to-shot fluctuation and transient heating of the detector. These two beams were then focused into an astigmatism-corrected spectrographic monochromator (SpectraPro-150, Acton Research Corp., 150 gv/mm, 4.0 μm blazed) to form two spectrally resolved images on a focal-plane-array (FPA) IR detector. The two frequency-resolved images were digitized by two windows of 12 × 200 pixels, which allowed simultaneous normalization of a ~70-cm^{-1} spectrum. The censoring chip of the detector was an engineering grade, (256 × 256)-element HgCdTe matrix of dimensions 1.28 × 1.28 cm^2 (or 50 × 50 μm^2 per pixels). During the course of an experiment, the sensing chip and its immediate circuits were kept in contact with a 4-L liquid nitrogen dewar to increase its sensitivity in the IR range. The long-time temperature drift was minimized by normalizing the gain against the FPA readouts from a small region far away from the illuminated area. Rejection of bad laser shots further improved the S/N ratio. With a data acceptance ratio of about 0.5 and a 30-Hz laser repetition rate, it took about 1 min to acquire signals on the order of 1% absorbance change with a 10:1 S/N ratio after signal averaging for 1000 valid laser shots. The typical spectral and temporal resolution for this setup were ~4 cm^{-1} and ~300 fs, respectively. The polarizations of the pump and the probe pulse were set at the magic angle (54.7°) to ensure that all signals were due to population dynamics. All kinetic data have been corrected for a positive chirp of ~1.4 fs/cm^{-1}, measured from pump−probe cross correlation with use of a silicon wafer. A broad, wavelength-independent background signal from CaF_2 windows has also been subtracted from the transient spectra and kinetic traces.

Nanosecond Step-Scan FTIR. These measurements were made by using a Step-Scan FTIR spectrometer described elsewhere.[31] The instrument was based on a Bruker IFS-88 FTIR with a special scanner module to allow step scanning. An InSb detector with a 40-ns temporal full-width-half-maximum (fwhm) measured from the IR scatter of 1064-nm light from a YAG laser was used. The IR light was focused in the cavity with two 10-mm focal length BaF_2 lenses, which gave beam sizes smaller than comparable curved mirrors, allowing increased IR throughput. The sample was photoexcited with 10-ns pulses at 295 nm from the second harmonic of a dye laser.

Theoretical. To represent the chemical species in a practically tractable way, the solvent molecule in the complexes $Re_2(CO)_9$(solvent) was represented by CH_4 for alkane or by CH_3Cl for solvation through the Cl atom in halogenated solvents. For density-functional theoretical (DFT) calculations, the commercial JAGUAR package was used.[32] The exchange-correlation functional employed was the Becke's three-parameter hybrid functional[33] combined with the Lee−Yang−Parr (LYP) correlation functional,[34] commonly denoted as B3LYP.[35] This functional has been shown to give very good results for transition metal complexes.[36,37] Except for molecules with apparent symmetry such as CH_4 or $Re_2(CO)_{10}$, no constraint was imposed during geometry optimization. The basis set consisted of the 6-31G basis functions for H, C, O, and Cl atoms,[38,39] and the Los Alamos Effective Core Potential

(23) Stiegman, A. E.; Tyler, D. R. *Comments Inorg. Chem.* **1986**, *5*, 215.
(24) Tyler, D. R. *Acc. Chem. Res.* **1991**, *24*, 325.
(25) Baird, M. C. *Chem. Rev.* **1988**, *88*, 1217.
(26) Yang, H.; Snee, P. T.; Kotz, K. T.; Payne, C. K.; Frei, H.; Harris, C. B. *J. Am. Chem. Soc.* **1999**, *121*, 9227.
(27) Harris, G. W.; Boeyens, J. C. A.; Coville, N. J. *Organometallics* **1985**, *4*, 914.
(28) Harris, G. W.; Coville, N. J. *Organometallics* **1985**, *4*, 908.
(29) Harris, G. W.; Boeyens, J. C. A.; Coville, N. J. *J. Chem. Soc., Dalton Trans.* **1985**, 2277.
(30) Lian, T.; Bromberg, S. E.; Asplund, M. C.; Yang, H.; Harris, C. B. *J. Phys. Chem.* **1996**, *100*, 11994.
(31) Sun, H.; Frei, H. *J. Phys. Chem. B* **1997**, *101*, 205.
(32) *Jaguar 3.5*; Schroedinger, Inc.: Portland, OR, 1998.
(33) Becke, A. D. *J. Chem. Phys.* **1993**, *98*, 5648.
(34) Lee, C.; Yang, W.; Parr, R. G. *Phys. Rev.* **1988**, *B41*, 785.
(35) Stephens, P. J.; Devlin, F. J.; Chabalowski, C. F.; Frisch, M. J. *J. Phys. Chem.* **1994**, *98*, 11623.
(36) Ricca, A.; Bauschlicher, C. W. *Theor. Chim. Acta* **1995**, *92*, 123.
(37) Glukhovtsev, M. N.; Bach, R. D.; Nagel, C. J. *J. Phys. Chem.* **1997**, *101*, 316.
(38) Francl, M. M.; Petro, W. J.; Hehre, W. J.; Binkley, J. S.; Gordon, M. S.; DeFrees, D. J.; Pople, J. A. *J. Chem. Phys.* **1982**, *77*, 3654.
(39) Hehre, W. J.; Ditchfield, R.; Pople, J. A. *J. Chem. Phys.* **1972**, *56*, 2257.

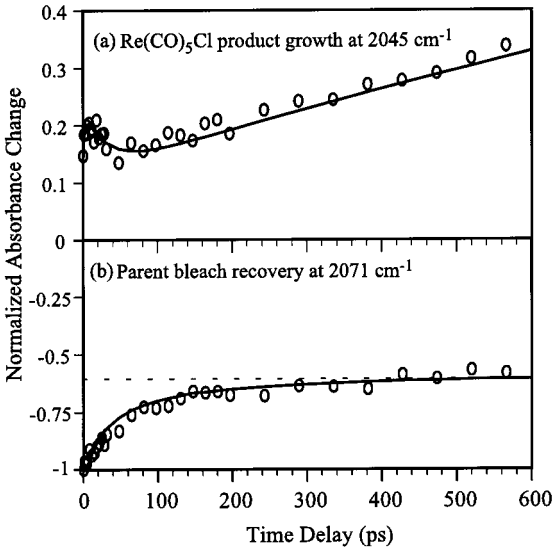

Figure 1. Ultrafast kinetics of $Re_2(CO)_{10}$ following 295-nm UV photolysis in CCl_4. The product kinetics in panel a were recorded at 2045 cm^{-1}. Parent bleach kinetics on panel b were recorded at 2071 cm^{-1}. Solids lines are simulations to a diffusion model for geminate-pair recombination (see text).

(ECP) for Re with the outermost core orbitals included in the valence description (ECP+5s5p6s5d6p).[40] To make certain that a proper energy extremum had been located each geometry optimization was followed by a frequency calculation at the same level of theory. The resulting frequency analyses were used to calculate thermodynamic properties such as the zero-point energy (ZPE) and enthalpy (H) at 298 K. The interaction energy between a metal fragment and a model solvent molecule was also calculated, using the counterpoise technique to account for basis set superposition error (BSSE).[41,42]

Results and Discussions

The Reaction Dynamics following Dissociation Pathway (i): Photolysis of the Re−Re Bond. It has been shown in a previous Communication that the $Re(CO)_5$ radical is only weakly solvated in alkane or chlorinated alkane solvents.[26] The interaction energies for $Re(CO)_5/CH_4$ and $Re(CO)_5/CCl_4$ have been calculated to be ca. −0.2 kcal/mol and ca. −0.6 kcal/mol, respectively.[43] The weak interaction allows the chemically active Re center to recombine with another $Re(CO)_5$ radical to form the parent $Re_2(CO)_{10}$ without much energy cost in displacing the solvent molecule. In the reactive CCl_4 solution, the parent $Re_2(CO)_{10}$ molecule exhibits two reformation time scales of ∼50 and ∼500 ps. The $Re(CO)_5$ radicals are also capable of abstracting a Cl atom from CCl_4 to form $Re(CO)_5Cl$ on a time scale of ∼1.3 ns. In this section, it will be shown that the competing geminate-recombination and Cl-atom abstraction are regulated by solvent caging, and that treating the solvent as a viscous continuum is sufficient to account for the observed dynamics.

The kinetic traces of the $Re(CO)_5Cl$ and $Re_2(CO)_{10}$ are reproduced in Figure 1. The biphasic recovery of the parent bleach shown in Figure 1b has been explained by a modified diffusion model in the literature.[44] For clarity, the model and required parameters are briefly restated below. The reaction is considered to follow the diffusion equation in a continuous medium,

$$\frac{\partial}{\partial t}w(r,t;r_0,R) = D\nabla^2 w(r,t;r_0,R) \qquad (2)$$

where $w(t,r;r_0,R)$ is the time-dependent survival probability density of a pair of monomers and D is the diffusion coefficient of the monomer in the solvent. The model assumes that a pair of $Re(CO)_5$ radicals rest at r_0 apart at time $t \rightarrow 0$. The two radicals can react to form $Re_2(CO)_{10}$ when their separation r is equal to or smaller than a critical distance R. To account for the finite recombination rate, an additional boundary condition at $r = R$ is imposed,

$$D\frac{\partial}{\partial t}w(r,t;r_0,R)_{r=R} = bw(r,t;r_0,R) \qquad (3)$$

Known as the "radiation boundary condition", eq 3 states that the recombination rate is proportional to the concentration at the contact distance R. The relation of the proportionality b in eq 3 to the recombination rate constant can be expressed by,

$$k_r = 4\pi R^2 b \qquad (4)$$

The physical parameters needed for the analysis of the experimental data are the branching ratio Q_i for pathway (i), the solvent viscosity η, the contact distance R, the initial separation r_0, and the recombination rate constant k_r. The contact distance R is assigned as twice the distance from the center of the Re−Re bond to the center of the axial Re−C−O line. Similar treatments for the contact distance have been employed in the analysis of geminate pair dynamics of disulfides.[45,46] By using the crystallographic data of $Re_2(CO)_{10}$,[47] R is estimated to be 6.3 Å. To verify this estimate, the DFT geometry for the $Re(CO)_5$ radical and the Lennard-Jones parameters for the C and O atoms are used to construct a Lennard-Jones $Re(CO)_5$ molecule suitable for classical molecular simulation.[48] The contact distance in this approach is defined as the diameter of a sphere that encloses the Lennard-Jones $Re(CO)_5$. This procedure gives a contact distance of 6.2 Å, consistent with the first estimate.

For the Cl-atom abstraction reaction in CCl_4 solution ($\eta_{20°C}$ = 0.97 cp), the product kinetics and parent bleach signal are fitted simultaneously since they both draw from the same $Re(CO)_5$ source. Three processes are considered to contribute to the observed product kinetics: vibrational cooling, nonequilibrium barrier crossing to form the product, and equilibrium barrier crossing. Incorporating these ideas, the normalized product signal is described as,

$$I_{\text{product}}(t) = A_{\text{vib}}\exp(-t/\tau_{\text{vib}}) + A_{\text{neq}}(1-\exp(-t/\tau_{\text{neq}})) + \int_0^t \mathrm{d}t' k_a M(t';r_0,R) \qquad (5)$$

The first term of eq 5 describes the relaxation of vibrationally excited low-frequency modes (hot bands) that overlap with the product band; the second term models the nonequilibrium product formation with a phenomenological rise time τ_{neq}, and the last term relates the time-dependent $Re(CO)_5$ concentration $M(t;r_0,R) = \int_R^\infty \mathrm{d}r 4\pi r w^2(r,t;r_0,R)$ to the macroscopic, pseudo-

(40) Hay, P. J.; Wadt, W. R. *J. Chem. Phys.* **1985**, *82*, 299.
(41) Boys, S. F.; Bernardi, F. *Mol. Phys.* **1970**, *19*, 553.
(42) Liu, B.; McLean, A. D. *J. Chem. Phys.* **1973**, *59*, 4557.
(43) The basis set used in these calculations was augmented by placing polarization functions on all atoms except Re.
(44) Naqvi, K. R.; Mork, K. J.; Waldenstrfm, S. *J. Phys. Chem.* **1980**, *84*, 4, 1315.
(45) Scott, T. W.; Liu, S. N. *J. Phys. Chem.* **1989**, *93*, 1393.
(46) Bultmann, T.; Ernsting, N. P. *J. Phys. Chem.* **1996**, *100*, 19417.
(47) Churchill, M. R.; Amoh, K. N.; Wasserman, H. J. *J. Inorg. Chem.* **1981**, *20*, 1609.
(48) Straub, J. E.; Karplus, M. *Chem. Phys.* **1991**, *158*, 221.

first-order rate constant k_a. To account for the nonequilibrium barrier crossing in the CCl_4 case, the normalized parent signal can be written as,

$$I_{\text{parent}}(t) = -1 + (1 - A_{\text{neq}}) \times Q_i \times \int_0^t \mathrm{d}t' 4\pi R^2 b w(r = R, t'; r_0, R) \quad (6)$$

With R fixed (=6.256 Å) and Q_i (=0.8) obtained from experiments, the recombination rate is found to be $k_r = (1.0 \pm 0.2) \times 10^{11}$ M^{-1} s^{-1}, an order of magnitude greater than the literature value measured in CH_3CN, $(1.0 \pm 0.2) \times 10^{10}$ M^{-1} s^{-1}.[49] This is not surprising since in the current simplified model, a single parameter k_r is used to encompass all fast dynamics such as nondissociative energy relaxation and primary geminate-recombination. The initial separation of the two $Re(CO)_5$ monomers was found to be $r_0 = 8.6 \pm 0.2$ Å, about 2.3 Å away from their contact distance. The Cl-atom abstraction rate $k_a = (7.5 \pm 0.4) \times 10^8$ s^{-1} ($(7.3 \pm 0.4) \times 10^7$ M^{-1} s^{-1}) is in very good agreement with the literature value, which is calculated to be $(1.8-9.1) \times 10^7$ M^{-1} s^{-1} from a set of Arrhenius parameters.[50] The time constant for the fast rise of product kinetics τ_{neq} is found to be approximately 2−3 ps, with an amplitude $A_{\text{neq}} = 0.10 \pm 0.01$. That is, about 10% of the product is produced through nonequilibrium barrier crossing. Finally, the hot band intensity A_{vib} is found to be 0.13 ± 0.01 with a vibrational-cooling time $\tau_{\text{vib}} = 35 \pm 14$ ps. The resulting traces for the product and parent kinetics are plotted on top of the experimental data displayed in Figure 1.

Within the framework of the diffusion model, the physical origin of the experimental observation is illustrated in Figure 2. In Figure 2, the abscissa is the separation of the two $Re(CO)_5$ monomers, in units of Å. The equilibrium Re−Re distance $R_{\text{eq}} \sim 3.0$ Å, the contact distance $R \sim 6.3$ Å, and the initial separation $r_0 \sim 8.6$ Å are also marked. The portion to the left of R is a schematic potential energy surface plot depicting dynamics that are not susceptible to the current model. To the right of R are plots of the spatial distribution of a monomer around a recombination center at various time delays. At short time delays such as 1 and 5 ps, the distribution maxima still linger around the initial separation r_0. By comparing the 8.6-Å initial separation with the Lennard-Jones radius of CCl_4 of 5.8 Å, one can envision that following photodissociation the monomers are trapped in the first solvent shell for a few picoseconds. Furthermore, the initial distribution also broadens significantly on the 1−5 ps time scale. The broadening results in a fast buildup of the monomer concentration at R. Recall that the recombination rate k_r is defined to be proportional to the concentration at the contact distance R (eq 3). Consequently, the fast broadening of the distribution contributes to the experimentally observed fast recovery of the parent bleach. Driven by the accumulating population around R, the distribution diffuses away from the recombination center until the system reaches equilibrium. This is shown in Figure 2 for time delays longer than ca. 20 ps, where the distribution maximum starts to diffuse away noticeably. This diffusion process is identified with the longer recovery in the parent bleach data.

The Reaction Dynamics following Dissociation Pathway (ii): Photolysis of the Equatorial Re−CO Bond. The infrared spectra in the CO stretch region are presented in the form of difference absorbance in which positive bands indicate the appearance of new species while negative bands (bleaches) represent the depletion of parent molecules. In the stronger coordinating CCl_4 solution, the 1945, 1985, 1998, 2005, and 2055 cm^{-1} bands are assigned to the equatorially solvated nonacarbonyl species *eq*-$Re_2(CO)_9(CCl_4)$.[26] The CO stretching peaks of $Re(CO)_5Cl$ also appear on the ultrafast spectra as a result of Cl-atom abstraction. The nonacarbonyl solvate *eq*-$Re_2(CO)_9(CCl_4)$ is found to be stable up to the experimental time window of 2.5 μs.

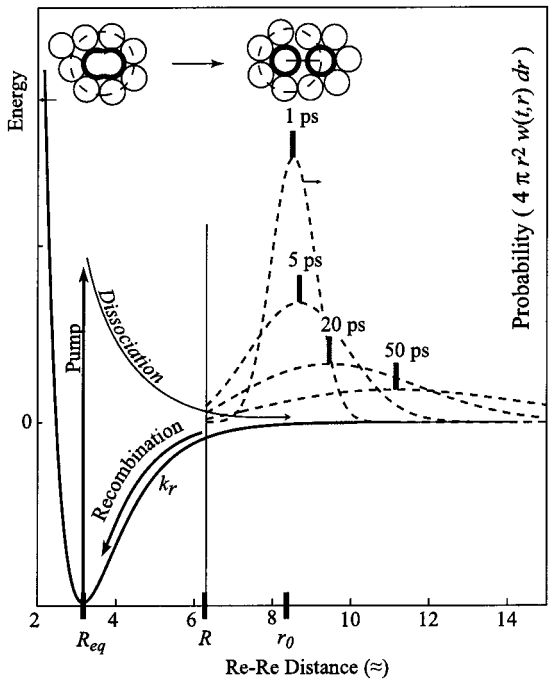

Figure 2. Illustration of the diffusion model for geminate recombination. On the abscissa, R_{eq} is the equilibrium Re−Re bond length of $Re_2(CO)_{10}$, R the contact distance, and r_0 the initial separation of the two $Re(CO)_5$ monomers. The schematic potential curve for the ground-electronic state and for the dissociative excited state are on the left. In this simplified model, the rate constant k_r encompasses energy relaxation processes resulting from nondissociative energy relaxation and primary geminate recombination. Time evolution of the probability distributions (dashed curves) for the geminate pair are on the right. Inset: An illustration of solvent caging. The thick circles represent the $Re(CO)_5$ monomers and the thin circles CCl_4 molecules. A dashed circle roughly shows the extent of the first solvent shell.

In the weaker coordinating hexane solution, the early-time spectra (for example, the 10-ps panel of Figure 3) are typically broad and featureless which results from spectral overlap and excitation of low-frequency bands.[51,52] As the photoproducts dissipate excess vibrational energy at later time delays, the IR bands narrow in and rise to reveal several identifiable bands. For the $Re_2(CO)_{10}$ molecules that dissociate though channel (i) in eq 1, the nascent $Re(CO)_5$ radicals appear as the most intense broad peak centering on 1992 cm^{-1} in the 660-ps panel of Figure 3. This assignment is in very good agreement with the previously reported $Re(CO)_5$ band (1990 cm^{-1}) in cyclohexane solution.[16] On the basis of matrix-isolation experiments, the peaks at 1942, 1973, 1984, 1999, and 2051 cm^{-1} on the same panel are attributed to the equatorially solvated dirhenium nonacarbonyl *eq*-$Re_2(CO)_9$(hexane),[17] in which a solvent molecule occupies the equatorially vacant site left behind by the leaving CO ligand. The kinetic trace of *eq*-$Re_2(CO)_9$(hexane) at 2051 cm^{-1} exhibits a single-exponential rise of 69 ± 5 ps and is attributed to

(49) Sarakha, M.; Ferraudi, G. *Inorg. Chem.* **1996**, *35*, 313.
(50) Meckstroth, W. K.; Reed, D. T.; Wojcicki, A. *Inorg. Chim. Acta* **1985**, *105*, 147.
(51) Dougherty, T. P.; Heilweil, E. J. *Chem. Phys. Lett.* **1994**, *227*, 19.
(52) Arrivo, S. M.; Dougherty, T. P.; Grubbs, W. T.; Heilweil, E. J. *Chem. Phys. Lett.* **1995**, *235*, 247.

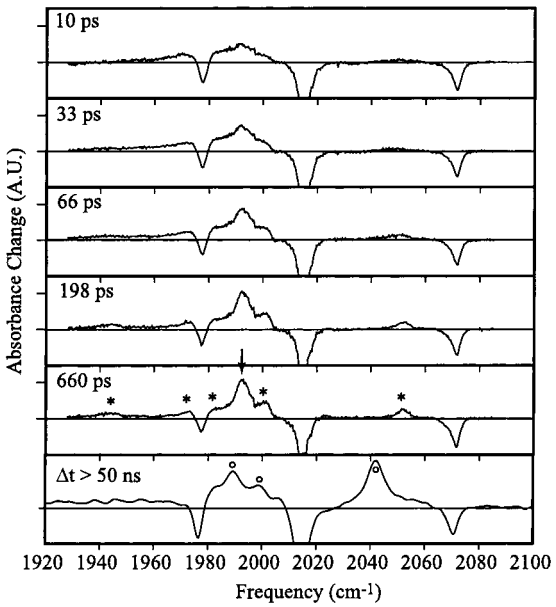

Figure 3. Transient difference spectra in the CO stretching region for $Re_2(CO)_{10}$ in hexane solution at 10, 33, 66, 198, and 660 ps following 295-nm UV photolysis. The last panel is an averaged spectrum for pump−probe delay greater than 50 ns. The equatorially solvated *eq*-$Re_2(CO)_9$(hexane) is indicated by asterisks, and the $Re(CO)_5$ radical is marked by an arrow. IR bands due to the proposed $[eq\text{-}Re_2(CO)_9]^{bare}$ are marked by open circles. It is very likely, however, that the last panel is a spectrum of $[eq\text{-}Re_2(CO)_9]^{bare}$ and *eq*-$Re_2(CO)_9$(hexane) in equilibrium, considering the similar stability of the two species (see main text). No discernible spectral features were observed in the region 2080−2130 cm^{-1} (not shown).

vibrational relaxation of the binuclear *eq*-$Re_2(CO)_9$(hexane) complex. As indicated by the nanosecond spectra in Figure 3, the *eq*-$Re_2(CO)_9$(hexane) solvate is stable on the ultrafast time scale up to ∼1 ns. But at longer time delays (>50 ns), the *eq*-$Re_2(CO)_9$(hexane) thermally transforms to another species that has discernible CO stretches at 1990, 1999, and 2043 cm^{-1} as shown in the last panel of Figure 3. This species is assigned as unsolvated *eq*-$Re_2(CO)_9$, denoted $[eq\text{-}Re_2(CO)_9]^{bare}$, based on theoretical considerations to be discussed below. Although the current experimental setup does not permit an accurate measurement of the transformation rate from the solvated *eq*-$Re_2(CO)_9$(hexane) to the unsolvated $[eq\text{-}Re_2(CO)_9]^{bare}$, the time constraints (1 ns < rate < 50 ns) allow for an evaluation of the lower and upper bounds of the free-energy barrier, which is estimated to be $5.2 < \Delta G^{\ddagger} < 7.5$ kcal/mol.

Quantum-Chemical Characterizations, Geometry Optimization. A series of DFT calculations were carried out in efforts to identify and further characterize the transient species that appear in the time-resolved IR spectra. Shown in Figure 4 are the optimized structures[53] of the parent molecule $Re_2(CO)_{10}$ and the unsolvated $Re(CO)_5$ and $Re_2(CO)_9$. Compared to X-ray diffraction data,[47] the calculations reproduce reasonably well the Re−C bond lengths in $Re_2(CO)_{10}$, which are on the average about 0.02 to 0.03 Å longer than experimental values. When the dissociation proceeds through pathway (ii) in eq 1, the resulting coordinatively unsaturated $Re_2(CO)_9$ can assume two different conformations that belong to different symmetry point groups. The structure of the *ax*-$Re_2(CO)_9$ conformer is located by removing an axial CO ligand from $Re_2(CO)_{10}$ as the initial guess for geometry optimization. The other *eq*-$Re_2(CO)_9$ conformer is located by removing an equatorial CO ligand from

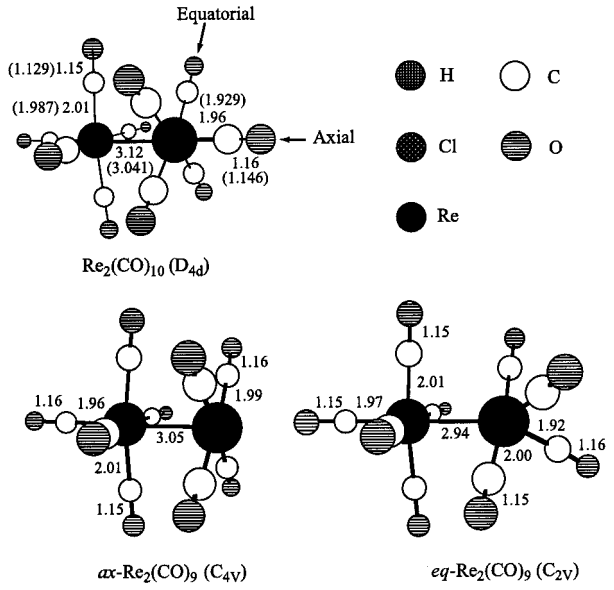

Figure 4. Schematic representations of $Re_2(CO)_{10}$, *ax*-$Re_2(CO)_9$, and *eq*-$Re_2(CO)_9$. Important geometrical parameters (in Å) and symmetry groups are also shown in the figure. Experimental values are included in parentheses.[47]

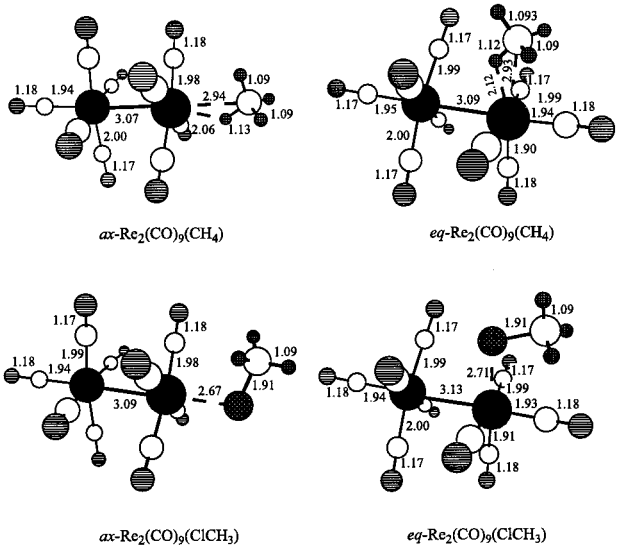

Figure 5. Schematic representations of *ax*-$Re_2(CO)_9(CH_4)$, *eq*-$Re_2(CO)_9(CH_4)$, *ax*-$Re_2(CO)_9(ClCH_3)$, and *eq*-$Re_2(CO)_9(ClCH_3)$. Important geometrical parameters (in Å) are also shown in the figure.

$Re_2(CO)_{10}$ as the initial guess. For the addition of alkanes, the structures of *ax*-$Re_2(CO)_9(CH_4)$ and *eq*-$Re_2(CO)_9(CH_4)$ are displayed in Figure 5. Generally, the methane molecule in both complexes interacts with one metal center in a side-on fashion,[54] and exhibits an extended (∼0.04 Å) C−H bond at the binding site. Figure 5 shows the configurations of solvated *ax*-$Re_2(CO)_9(ClCH_3)$ and *eq*-$Re_2(CO)_9(ClCH_3)$. In both complexes, the CH_3Cl molecule appears to interact with the nonacarbonyl through the Cl atom. It should be noted that the calculated "bare" dirhenium fragment of *eq*-$Re_2(CO)_9$ exhibits a marked difference in geometry compared to those of *eq*-$Re_2(CO)_9(CH_4)$ or *eq*-$Re_2(CO)_9(ClCH_3)$. In particular, without a solvent coordination in the equatorial position, the most stable structure of $Re_2(CO)_9$ appears to assume a local C_{2v} symmetry at the coordinatively unsaturated Re site as shown in Figure 4. This observation suggests that the bare *eq*-$Re_2(CO)_9$ fragment must reorganize

(53) Bode, B. M.; Gordon, M. S. *J. Phys. Chem. A* **1998**, *1997*, 4646.

(54) Zaric, S.; Hall, M. B. *J. Phys. Chem. A* **1997**, *101*, 4646.

Table 1. Summary of Relative Stability of the Axial and Equatorial Conformers at Various Levels of Theory[a]

	B3LYP	B3LYP + ΔZPE
$Re_2(CO)_9$	16.9	16.3
$Re_2(CO)_9(CH_4)$	10.8	10.1
$Re_2(CO)_9(ClCH_3)$	11.1	11.0

[a] In the table, ΔZPE is the zero-point energy correction. The energies shown here correspond to $(E_{ax} - E_{eq})$ in units of kcal/mol.

before accommodating a solvent molecule. That is, a reorganization energy barrier exists for the solvation process:

$$eq\text{-}Re_2(CO)_9 + \text{solvent} \rightarrow eq\text{-}Re_2(CO)_9(\text{solvent}) \quad (7)$$

Quantum-Chemical Characterizations, Energetics. One next turns to the energetics of the species discussed above. The relative stability of the axial and equatorial form of dirhenium complexes is summarized in Table 1. The unsolvated *eq*-$Re_2(CO)_9$ is energetically 16.3 kcal/mol more stable than the unsolvated *ax*-$Re_2(CO)_9$, in accordance with the proposition that the electronic effect is the dominating factor for equatorial substitution in $Re_2(CO)_9$ complexes.[27] Such electronic influence is somewhat lessened after solvation, as indicated by the 10.1 and 11.0 kcal/mol *ax* to *eq* stabilization energies for $Re_2(CO)_9(CH_4)$ and $Re_2(CO)_9(ClCH_3)$, respectively. The decrease in the $(E_{ax} - E_{eq})$ energy gap upon solvation (−6.2 or −5.3 kcal/mol) can be understood by two factors: the energy requirement for the aforementioned structural reorganization and the energy cost due to steric interaction of the solvent molecule and the metal fragment. While the steric interaction is difficult to evaluate with these calculations, the reorganization energy can be estimated by $(E^{sol} - E^{bare})$, where E^{bare} is the energy of the optimized, unsolvated dirhenium fragment *ax*-$Re_2(CO)_9$ (or *eq*-$Re_2(CO)_9$) and E^{sol} is the energy of the dirhenium fragment at the solvated geometry. Calculations show that there is almost no energy difference (<0.3 kcal/mol) for the conformational change in the dirhenium fragment from the unsolvated $[ax\text{-}Re_2(CO)_9]^{bare}$ to the axially solvated form $[ax\text{-}Re_2(CO)_9]^{sol}$ in either $ClCH_3$ or CH_4. On the other hand, a minimum energy of 5.5 or 7.1 kcal/mol is required for the unsolvated $[eq\text{-}Re_2(CO)_9]^{bare}$ to rearrange to the equatorially solvated form $[eq\text{-}Re_2(CO)_9]^{sol}$ in CH_4 or CH_3Cl, respectively.[55] The results suggest that the energy requirement for structural reorganization contributes significantly to the reduction of the $(E_{ax} - E_{eq})$ energy gap upon solvation.

To examine whether the solvation energy is sufficient to compensate for structural reorganization, the binding energies for *ax*- and *eq*-$Re_2(CO)_9$...(solvent) are also calculated and summarized in Table 2. One sees in Table 2 that the binding energies for *ax*- and *eq*-$Re_2(CO)_9$...(CH_4) are similar in magnitude; however, the energy cost for structural reorganization of the equatorially solvated species (5.5 kcal/mol) is approximately equal to the equatorially solvated species' binding energy. As a result, the overall binding energy of *eq*-$Re_2(CO)_9$...(CH_4) is on the order of 1−2 kcal/mol. Table 2 also shows that the binding energy of *eq*-$Re_2(CO)_9$...$(ClCH_3)$ is about 9 kcal/mol greater than that of *eq*-$Re_2(CO)_9$...(CH_4), providing a qualitative rationale for experimental observations that the equatorial solvate *eq*-$Re_2(CO)_9(ClCCl_3)$ is stable up to the experimental window 2.5 μs. The calculations predict their relative stability of dirhenium nonacarbonyl solvates to be, in order of increasing stability, *ax*-$Re_2(CO)_9 \ll ax$-$Re_2(CO)_9(CH_4) < ax$-$Re_2(CO)_9(ClCH_3) \approx eq$-$Re_2(CO)_9 \approx eq$-$Re_2(CO)_9(CH_4) \ll eq$-$Re_2(CO)_9(ClCH_3)$. The relative stability of the *ax*-$Re_2(CO)_9(CH_4)$ and *eq*-$Re_2(CO)_9(CH_4)$, the weak binding energy of *eq*-$Re_2(CO)_9(CH_4)$, and an estimated minimal barrier of 6−7 kcal/mol for solvation of *eq*-$Re_2(CO)_9$ with CH_4 lead one to propose the unsolvated *eq*-$Re_2(CO)_9$ as the thermodynamically more stable species in hexane solution.

(55) The barrier to solvation is likely to be equal to or greater than the difference in energy between the two conformations. The relaxation energies of the CH_4 and CH_3Cl complexed fragments do not contribute significantly to the total relaxation energy (<1 kcal/mol) and are thus not included.

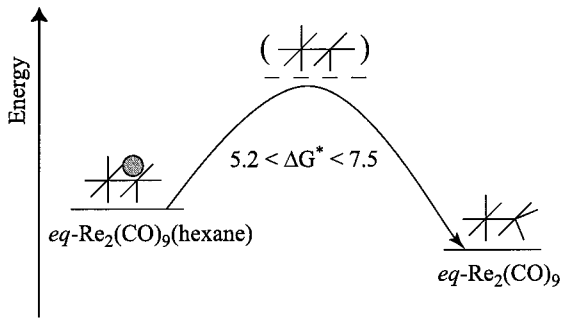

Figure 6. An illustration of structural reorganization in equatorial solvation. The structure above the solid arrow connecting *eq*-$Re_2(CO)_9$(hexane) and *eq*-$Re_2(CO)_9$ demonstrates schematically the structural deformation of the $Re_2(CO)_9$ fragment and the associated energy cost. Note that it does not represent the transition-state structure nor does the solid line indicate the actual reaction pathway.

Proposed Solvation Process. Within the context of the unsolvated *eq*-$Re_2(CO)_9$ being the most stable species, the experimental observations are explained in Figure 6. Photodissociation of an equatorial CO ligand creates a coordinatively vacant site at the metal, which is quickly occupied by a solvent molecule in the dense liquid environment within a few picoseconds to form the *eq*-$Re_2(CO)_9$(hexane) solvate. The equatorial solvate then vibrationally cools on a time scale of 69 ps. The vibrationally cooled equatorial solvate is stable on the ultrafast time scale (<1 ns), but transforms to the unsolvated *eq*-$Re_2(CO)_9$ within 50 ns after photolysis. That is, the hexane solvate may traverse a free-energy barrier in the range of $5.2 < \Delta G^{\ddagger} < 7.5$ kcal/mol to become an unsolvated *eq*-$Re_2(CO)_9$. The theoretically estimated reorganization energy of 6−7 kcal/mol provides a reasonable rationale for the minimum free-energy barrier, although the nature of the transition state is not clear at this point. The experimentally observed greater stability of *eq*-$Re_2(CO)_9(CCl_4)$ over *eq*-$Re_2(CO)_9$(hexane) then can be understood by the much greater solvation energy exhibited by *eq*-$Re_2(CO)_9(CCl_4)$.

Conclusion

The ultrafast events that follow 295-nm photolysis of $Re_2(CO)_{10}$ have been studied in detail in the reactive, stronger-coordinating CCl_4, and in the inert, weaker-coordinating hexane solutions. The experimental results for the $Re_2(CO)_{10}/CCl_4$ system show that 22.5% of the initially excited $Re_2(CO)_{10}$ molecules dissociate to $Re(CO)_5$ radicals that are able to escape cage recombination and abstract a Cl atom from the CCl_4 solvent. About 2.5% of the excited $Re_2(CO)_{10}$ molecules dissociate to form $Re(CO)_5$ radicals and react further to cross the energy barrier to abstract a Cl atom on a time scale faster than vibrational cooling. Such a nonequilibrium barrier crossing can be understood by considering the excess energy the initiation UV photon deposits on the $Re(CO)_5$/solvent system. About 20% of the excited $Re_2(CO)_{10}$ molecules dissociate through a Re−CO_{eq} bond to form the equatorial solvate, *eq*-$Re_2(CO)_9(CCl_4)$, which is stable up to the experimental time window of 2.5 μs. Finally, about 55% of the excited parent molecules reverted to

Table 2. Summary of the Binding Energies[a]

	ax-$Re_2(CO)_9(CH_4)$	*eq*-$Re_2(CO)_9(CH_4)$	*ax*-$Re_2(CO)_9(ClCH_3)$	*eq*-$Re_2(CO)_9(ClCH_3)$
B3LYP				
ΔE	−6.7	−0.5	−15.1	−9.3
$\Delta E + \Delta$ZPE	−7.7	−1.0	−15.8	−10.0
$\Delta E + \Delta$ZPE $+ \Delta H$	−7.7	−2.1	−15.4	−10.7
CP	−6.1	−5.2	−13.5	−14.3
CP + ΔZPE	−7.0	−5.7	−14.1	−14.9
CP + ΔZPE + ΔH	−7.0	−6.7	−13.8	−15.6

[a] Note that the structural reorganizational energies for the $Re_2(CO)_9$ fragments are not included. See the text. In the table, ΔZPE is the zero-point energy correction, ΔH is the correction term for finite temperature (298 K) enthalpy, and CP is the counterpoise procedure for correcting the basis set superposition error.

their electronic ground state, either via an internal relaxation or through geminate recombination.

In hexane solution, the recombination of $Re(CO)_5$ radicals is also regulated by solvent caging but without the competing channel of atom abstraction as in the case of CCl_4. Following dissociation pathway (ii), the equatorial solvate *eq*-$Re_2(CO)_9$-(hexane) is found to further react to form another species on a time scale between 1 and 50 ns, or equivalently a free-energy requirement of 5.2 to 7.5 kcal/mol. With the aid of quantum-chemical calculations, this thermodynamically more stable species is attributed to the unsolvated *eq*-$Re_2(CO)_9$. In this picture, the energy requirement can be understood to stem from the necessary structural rearrangement for *eq*-$Re_2(CO)_9$ to accommodate a solvent molecule in the equatorial position.

This work may suggest that for metal radical species the solvent can be treated as a viscous continuum, whereas for the dinuclear complexes the solvent is best described in molecular terms. This conclusion together with the notion of reorganization-solvation may help to better understand the roles of solvent in photoactivation of multinuclear organometallic compounds.

Acknowledgment. This work was supported by a grant from the National Science Foundation. The Office of Basic Energy Science, Chemical Science Division, U.S. Department of Energy contract No. DE-AC03-76FS00098 is acknowledged for specialized equipment used in the course of these experiments. The authors thank H. Frei for the use of the step-scan FTIR spectrometer and helpful discussions, and A. Rizvi for his assistance with experiments.

Supporting Information Available: The Cartesian coordinates for structures optimized at the DFT-B3LYP level of theory (PDF). This material is available free of charge via the Internet at http://pubs.acs.org.

JA003344Y